SCIENTIFIC REPORTS

OPEN

SUBJECT AREAS:
HIGH-THROUGHPUT SCREENING
VIRTUAL DRUG SCREENING

Received
20 August 2014

Accepted
20 October 2014

Published
10 November 2014

Correspondence and requests for materials should be addressed to R.B. (baskaran.rajasekaran@gmail.com)

* These authors contributed equally to this work.

Identification of novel tyrosine kinase inhibitors for drug resistant T315I mutant BCR-ABL: a virtual screening and molecular dynamics simulations study

Hemanth Naick Banavath[1]*, Om Prakash Sharma[2]*, Muthuvel Suresh Kumar[2] & R. Baskaran[1]

[1]Department of Biochemistry & Molecular biology, School of Life Sciences, Pondicherry University-India, [2]Centre for Bioinformatics, School of Life Sciences, Pondicherry University-India.

BCR-ABL tyrosine kinase plays a major role in the pathogenesis of chronic myeloid leukemia (CML) and is a proven target for drug development. Currently available drugs in the market are effective against CML; however, side-effects and drug-resistant mutations in BCR-ABL limit their full potential. Using high throughput virtual screening approach, we have screened several small molecule databases and docked against wild-type and drug resistant T315I mutant BCR-ABL. Drugs that are currently available, such as imatinib and ponatinib, were also docked against BCR-ABL protein to set a cutoff value for our screening. Selected lead compounds were further evaluated for chemical reactivity employing density functional theory approach, all selected ligands shows HLG value > 0.09900 and the binding free energy between protein-ligand complex interactions obtained was rescored using MM-GBSA. The selected compounds showed least ΔG score -71.53 KJ/mol to maximum -126.71 KJ/mol in both wild type and drug resistant T315I mutant BCR-ABL. Following which, the stability of the docking complexes were evaluated by molecular dynamics simulation (MD) using GROMACS4.5.5. Results uncovered seven lead molecules, designated with Drug-Bank and PubChem ids as DB07107, DB06977, ST013616, DB04200, ST007180 ST019342, and DB01172, which shows docking scores higher than imatinib and ponatinib.

Chronic myeloid leukemia (CML) arises due to the chromosomal aberration in which reciprocal translocation of the Abelson gene on chromosome 9 to break-point cluster region gene on chromosome 22 results in the creation of fusion oncogene, *bcr-abl* (9; 22) (q34; q11)[1]. The product of *bcr-abl* oncogene, BCR-ABL protein is a constitutively active tyrosine kinase that drives the disease CML through phosphorylation of many downstream effector molecules, including Grb2, RAK, ROS, PI3K, JNK, STAT5, AKT and Myc which consequently promoting cell proliferation[2,3]. Imatinib is the first FDA approved tyrosine kinase inhibitor (TKI) that has shown potent inhibitory effect on the progression of CML[4]. Despite imatinib's clinical success, resistance due to mutations and side effects are still a limitation of this drug[5]. To overcome resistance, second generation TKI's inhibitors, nilotinib[6] and dasatinib[7] were developed. However, neither compound effectively inhibits T315I mutant BCR-ABL, which constitutes 20% of all BCR-ABL mutations[8–10].

Ponatinib is the only available drug that is designed to overcome T315I gatekeeper mutation[11] and is efficient in inhibiting the mutant BCR-ABL[12]. Ponatinib exhibits triple carbon-carbon (ethynyl linkage) bond between the methyl phenyl and purine groups[13,14]. It holds the Isoleucine side chain without steric interference and without any loss of hydrogen bond (H_bond)[11]. It also showed similar binding pattern (DFG-out) as imatinib and nilotinib which interacts with Met318, Asp381 and the side chain of Glu286. In addition, the drug makes van der Waals contacts with Tyr253 and Phe382 because of squeezed conformation of the P-loop and DFG-out mode of activation loop respectively[14]. Despite potent inhibition capability, ponatinib shows severe side-effects like blood clotting in cardiac valves, chambers and cerebral vessels consequently leading to adverse conditions like myocardial infarction, cardiac stroke and cerebral infraction[15]. Therefore, a broad spectrum drug capable of inhibiting both wild-type and mutant BCR-ABL with fewer side effects is currently in demand. The availability of 3D-structure of the target protein and the structural details of ponatinib and T315I mutant BCR-ABL protein complex renders an opportunity to identify the most active drug candidate that can efficiently block the catalytic activity of BCR-ABL.

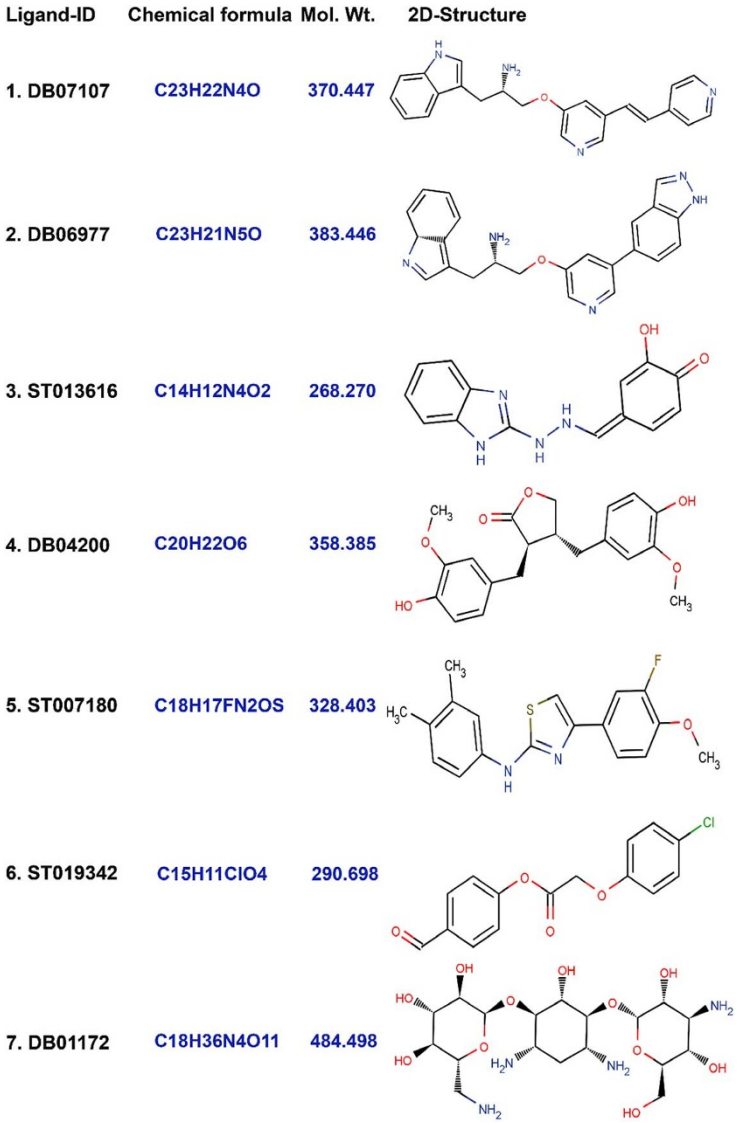

Figure 1 | 2-D Structures of the finally selected seven lead molecules have been shown in the figure. (1) DB07107, (2) DB06977, (3) ST013616, (4) DB04200, (5) ST007180, (6) ST019342, and (7) DB01172.

Table 1 | Glide XP results for the existing drug molecules with mutant and wild-type of BCR-ABL (T315I), by Schrödinger 9.3

Pubchem ID	Compound Name	Docking Score	HD:HA(Å)
Mutant type of BCR-ABL (T315I)			
24826799	Ponatinib	−11.917	Glu286:OE2::N3(2.865), Met318:N::N5 (2.815), Ile360:O::N2 (3.457), Asp381:N:: O1(2.867)
5328940	Bosutinib	−5.310	Asp381:OD2::n2(2.737), Ile360:N::N5 (3.047)
24853523	Bafetinib	−4.644	Asp381:O::N3(2.720), Arg362:nh2::n8 (3.223)
3062316	Dasatinib	−4.220	Ile360:O:O1(2.827), Arg362:NH1::O1(2.959) Ile360:N::O1(3.095)
644241	Nilotinib	−3.617	Arg362:NH1::O1(2.810), Asp381:OD2:N2 (3.029)
5291	Imatinib	−3.460	Glu292:OE2::N2(3.092), Ile360:O::N4 (3.027)
Wild-type of BCR-ABL			
24826799	Ponatinib	−10.285	Met318: H::N5(1.9), Asp381: H:: O1 (2.1), Glu286: OE2::H17 (2.3), Asp 381: OD2:: H17 (2.3), Asp 381: OD2::H28 (2.5)
5328940	Bosutinib	−7.462	Gly249: H::O3 (2.5), Asn322: HD21:N4 (2.0), Asn322: H:N4 (2.5)
24853523	Bafetinib	−10.188	Asp381: OD2::H32 (1.9), ASP 381:H::O1 (2.1), GLU286: OE2::H19 (2.1), THR315: OG1::H23 (2.5), ASN322: H::N8 (2.7)
3062316	Dasatinib	−7.574	GLU286: OE2::H15 (1.7)
644241	Nilotinib	−9.691	Asp381: H:: O1 (2.3), Glu286: OE2::N2 (1.8)
5291	Imatinib	−10.047	Asp381: OD2::N2(1.7), Asp381: H:: O1 (2.4), Glu 286: OE2::N3 (1.9)

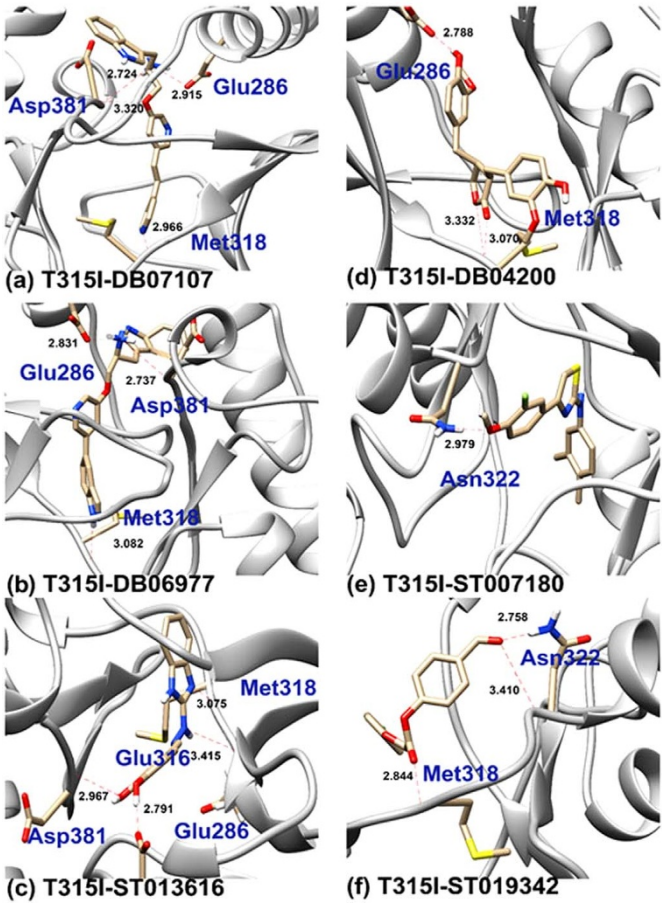

Figure 2 | Binding poses of the DB07107, DB06977, ST013616, DB04200, ST007180 and ST019342 lead molecules. The proposed binding mode of the lead molecules has been shown in the stick format. Residues involved in Hydrogen bonding have been labeled with the Hydrogen bond in dotted red lines and bond length have been shown in Angstrom.

Using a virtual screening approach, we have screened and identified potent drug-like compounds, efficient against both wild-type and mutant BCR-ABL, from a large library of small molecules. Drug molecules exhibiting docking score higher than ponatinib were manually explored in molecular visualization tools in order to analyze their binding patterns. Highest occupied molecular orbital (HOMO) and lowest unoccupied molecular orbital (LUMO) were calculated using DFT analysis to assess their chemical reactivity. Following which, protein-ligand complexes were incorporated in GROMACS for MD simulation to evaluate their structural stability throughout the trajectory period of simulation. Binding free energy for these complexes were then investigated to cross-check their binding affinity. Results of these studies uncovered seven lead molecules designated as DB07107, DB06977, ST013616, DB04200, ST007180 ST019342, and DB01172. Among these, DB07107, DB06977, ST013616, DB04200 and ST007180 were found to be more effective in blocking drug-resistant T315I mutant than the wild-type BCR-ABL. Interestingly ST019342, and DB01172 were effective only in mutant BCR-ABL.

Methods

Protein selection and preparation. The crystallographic co-ordinates for wild-type BCR-ABL (PDB ID: 3OXZ)[16] and mutant T315I (PDB ID: 3QRJ)[17] were retrieved from the Protein Data Bank (PDB). Prior to docking, protein structures were prepared by removing water molecules using Schrödinger software. Following which, bond orders were assigned, and hydrogen atoms were added to the crystal structures. Finally, a restrained minimization of the protein structure was performed using the default constraint of 0.30Å RMSD and the OPLS-2005 force field[18].

Ligand preparation and grid generation. A total of 36,481 small molecules were retrieved in Structure Data Format (SDF) from various small molecule libraries which includes Ligand.info: Small-molecule Meta-Database[19,20] (29,090), Drug Bank[21,22] (6,825) and PubChem[23] database (566). These small molecules were prepared using the LigPrep wizard of Schrödinger by assigning the bond orders and bond angles and then subjected to minimization using OPLS_2005 force field[18]. For accurate enumeration of ligand protonation states in biological condition we used Epik[24,25]. Then, Grid box of size 24 × 24 × 24 A^3 was generated keeping ATP binding site of BCR-ABL (Glu286, Met318, Ile360, Ala380, Asp381) as centroid using the "Receptor Grid Generation" of Schrödinger Glide[26].

Preparation of reference compounds. Reference compounds of FDA approved drugs such as ponatinib, bosutinib, bafetinib, dasatinib, nilotinib and imatinib were docked in the ATP binding site of both wild-type and mutant BCR-ABL. Ligands were prepared using the LigPrep module of Maestro followed by XP docking. The best docked complex score was set as the cutoff value for screening potential inhibitors of wild-type and mutant BCR-ABL.

Virtual screening. High throughput virtual screening (HTVS) was performed against the BCR-ABL using the Schrödinger software. Here, we used the virtual screening workflow of Glide Maestro for the docking. It performed the docking mainly in three phases namely, HTVS, SP (standard-precision) and XP (extra-precision). Using HTVS, we screened the large library of drug like molecules and reduced the intermediate conformations throughout the HTVS docking process. Successful compounds (10%) from HTVS were further assessed in SP docking for reliable docking of the screened compounds with high accuracy. To eliminate false-positive results, the best 10% of thriving compounds from SP docking were further incorporated for XP docking mode using advanced scoring.

Density functional theory analysis. Electronic effects of drug like molecules plays an important role in the pharmacological effects[27]. Therefore, drug candidates from the best binding poses were exported to Maestro 9.3 of Schrödinger 2012 version and geometry was optimized in the Jaguar panel using Becke's three-parameter exchange potential[28] and Lee-Yang-Parr correlation functional (B3LYP) theory[29,30] with 6-31G* basis set. Subsequently, surfaces (molecular orbital, density, potential) and atomic electrostatics potential charges (EPS) were monitored to compute the HOMO and LUMO. HOMO energy proposes the region of the small molecules, which can donate electron during the complex formation, while LUMO energy signifies the capacity of the molecule to accept the electrons from the partner protein. The difference in HOMO and LUMO energy, known as HOMO-LUMO gap energy, indicates the electronic excitation energy[31] that is necessary to compute the molecular reactivity and stability of the compounds[32].

Molecular dynamics simulations for protein ligand complexes. Two sets of Molecular Dynamics Simulations were performed using Gromacs 4.5.5[33]. In the first set, we evaluated the stability of the mutant type of BCR-ABL and selected the best seven drug candidates from the docking study. In the second set, we evaluated drug candidates with wild-type BCR-ABL. We used MD for performing protein and ligand complexes as described[34]. The topology file for the selected small molecules were generated using the automated topology builder (ATB)[35] in the framework of GROMOS 53A6 force-field[36]. The protein-ligand complexes were then solvated with TIP3P explicit water molecules and placed in the center of a cubic box of size 24 × 24 × 24 A^3. Minimum 1.0 Å distance was maintained between the protein and the edge of the simulation box so that protein can fully immerse with water and rotate freely. Then, Particle Mesh Ewald (PME) method[37] was used for the electrostatic energy calculation. It permits the use of the Ewald summation at a computational cost comparable to that of a simple truncation method of 10 Å or less, and the linear constraint solver (LINCS)[38] algorithm was used for covalent bond constraints. Before minimization, the system was neutralized by adding 8 Na^+ ions. The steepest descent approach (1000 ps) was used for each protein-ligand complex for energy minimization. Further NVT was performed for 100 ps to equilibrate the system with protein and ligand for constant volume, pressure (1 atm) and temperature (300 K). The final MD run was set to 10000 ps for each protein-ligand complex, and trajectories were saved for further analysis using Xmgrace and UCFC Chimera software[39].

Rescoring of BCR-ABL and drug candidate complexes using interaction energy and MM-GBSA approach. Interaction energy and Gibbs free energy were calculated using Gromacs and Schrödinger software. Interaction energy for BCR-ABL and drug complexes was calculated by estimating the short range Lennard-Jones and short range Coulomb energy using the g_energy analysis tool of Gromacs software.

$$E_{int} = E_{LJ} + E_{Coul} \quad (1)$$

Here, E_{int} stands for interaction energy, E_{LJ} stands for short ranges Lennard-Jones and E_{Coul} denotes short ranges for coulomb energy. It estimates the stability of proteins and drug candidate complexes. The binding free energy was calculated based on the following equation[40].

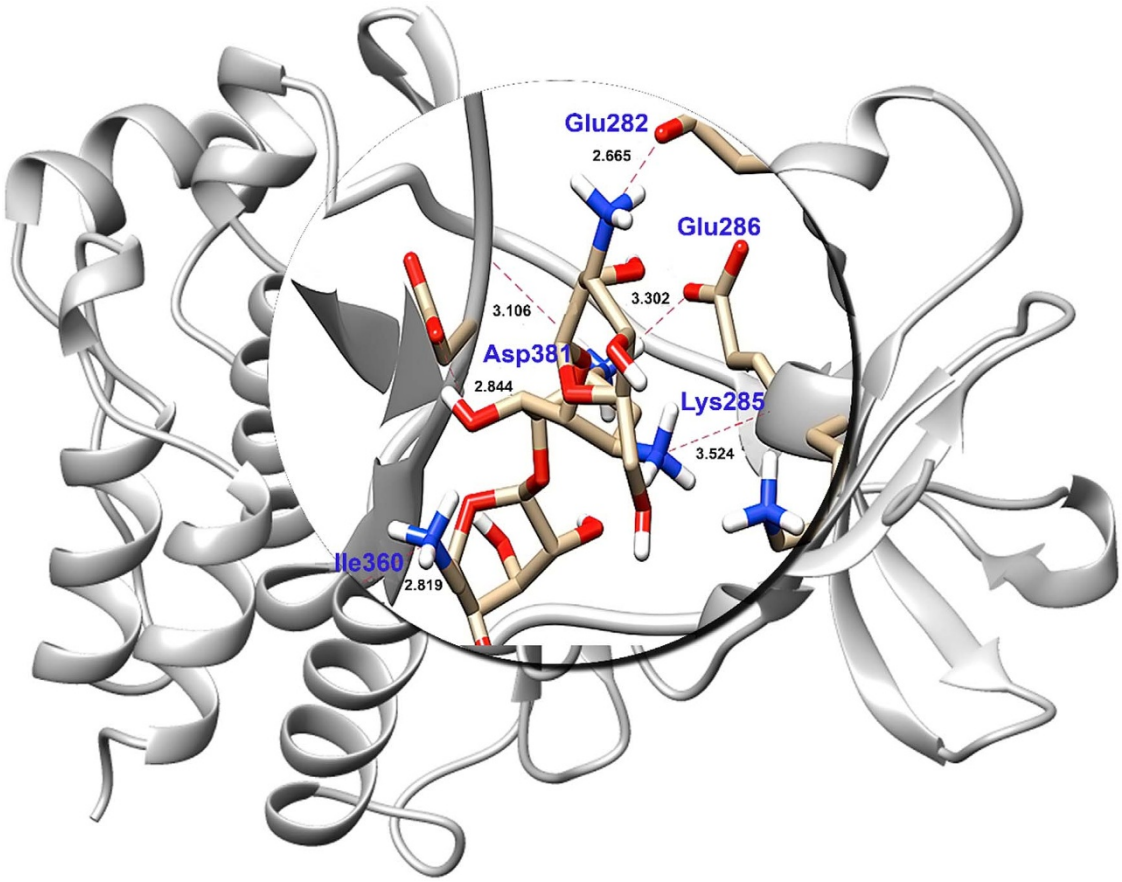

Figure 3 | Binding poses of the DB01172 lead molecule. The proposed binding mode of the lead molecules has been shown in the stick format. Residues involved in Hydrogen bonding have been labeled with the Hydrogen bond in dotted red lines and bond length have been shown in Angstrom.

Here, ΔEMM stands for the energy difference between ligands in complex and unliganded receptor.

$$\Delta G_{bind} = \Delta E_{MM} + \Delta G_{Solv} + G_{SA} \quad (2)$$

ΔGsolv is the difference in the G_{SA} solvation energy of the complex and the sum of solvation energy for the unbound ligand protein complex. ΔG_{Solv} is the difference in surface area energy for the complex and the sum of surface area energy for the protein and ligand.

Table 2 | Glide XP results for the seven lead molecules with the mutant (T315I) and wild-type of BCR-ABL, by Schrödinger 9.3

	Drug Bank ID	Docking Score	HD:HA(Å)
T315I mutant	**DB07107**	−14.031	Glu286:OE2:: N4(2.92), Met318:N:: N1 (2.97), Asp381:O1:: N(3.32), Asp381:N4:: O (2.72)
	DB06977	−13.163	Glu286:Oe2:: N5(2.81), Glu381:N5:: O (2.73), Met318:O:: N3(3.08)
	ST013616	−12.106	Glu286:OE2:: O1(2.79), Met381:O2:: O(2.96), Glu316:O: N2 (3.41), Met318:N:: N3(3.07)
	DB04200	−12.065	Glu286:OE2::O5(2.78), Met318: N:: O2 (3.07), Met318:N::O1(3.33)
	ST007180	−11.555	Asn322 ND2: O1 (2.79)
	ST019342	−11.033	Met318 N1: N (2.84), Asn322 N: O4 (3.41) Asn322 Nd2: O4 (2.75)
	DB01172	−8.603	Glu282 OE1: N4 (2.66), Lys285 O: N3 (3.52), Glu286 OE2: N2 (3.03), Ile360 O: N1 (2.82), Asp381 OD2: O4 (2.84), Asp381 O: N2 (3.10)
Wild-type	**DB07107**	−10.22	Glu286:Oe2::N2(2.658), Asp381:O::N2 (2.600), Asp381:N::O1(3.497), Met318:N:: N5(3.043)
	DB06977	−10.94	Asp381:O::N2(2.599), Glu286:Oe2::N2 (2.727)
	ST013616	−8.17	Lys 271:N2::O1(3.031), Glu286:Oe2::O2 (2.784), Glu286:Oe2::O1(2.627), Glu316: O::N2(3.228), Met318:N::N3(3.020)
	DB04200	−9.76	Met318:N::O1(3.177), Asn322:O3:: Nd2(2.972) Asp381:O::O6(2.915)
	ST007180	−9.62	Met318:O::N1(3.215), Met318:O:: S1(3.907)
	ST019342	−8.33	Met318:N::O2(3.016), Asn322:Nd2::O4 (3.129)
	DB01172	−9.72	Ile360:O::O8(2.900), Glu286:Oe2::N2(3.136), Asp381:N::O10 (2.787), Asp381: O::O10 (3.227), Asp381:Od2::O7(3.486), Glu286:Oe2::O3(2.963), His361:O::N4 (2.800), Asp381:Od2::Od2(2.647), Arg362:Nh1::O8 (3.365)

Table 3 | Frontier orbital energies of best seven lead compounds

Sl.No	Compound	HOMO (eV)	LUMO (eV)	HLG (eV)*
1.	DB07107	−0.29572	−0.14704	0.14868
2.	DB06977	−0.28270	−0.18359	0.09911
3.	ST013616	−0.18235	−0.06262	0.11973
4.	DB04200	−0.19362	−0.00920	0.18442
5.	ST007180	−0.18628	−0.03046	0.15582
6.	ST019342	−0.23036	−0.07439	0.15597
7.	DB01172	−0.57549	−0.40945	0.16604

Results and Discussion

Docking of reference compounds for HTVS. To set a cutoff value for docking studies, we docked all FDA approved drug such as ponatinib, bosutinib, bafetinib, dasatinib, nilotinib and imatinib using XP docking. Results showed that ponatinib has the highest binding affinity towards the T315I mutant BCR-ABL with a docking score of −11.050 kcal/mol while bosutinib, bafetinib, dasatinib, nilotinib and imatinib showed −5.513 kcal/mol, −4.689 kcal/mol, −4.702 kcal/mol, −3.772 kcal/mol, −3.593 kcal/mol and −3.78 kcal/mol, respectively (Table 1). Hence, for screening and identifying better lead molecules −11.00 kcal/mol was set as a cutoff value for XP docking.

Binding pose analysis of the identified compounds. Results of binding pose analysis of seven lead molecules with better binding affinity and higher binding free energy than the reference compounds. Four of which, designated DB07107, DB06977, DB04200 and DB0117, were from DrugBank and ST007180, ST013616 and ST019342 were from the ligand.info database. The 2D conformations and drug details are given in (Figure 1).

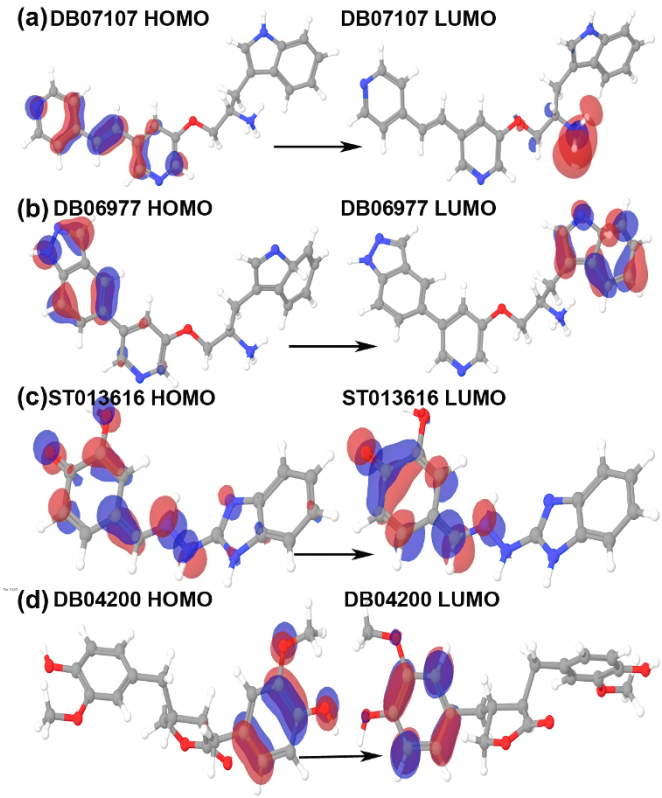

Figure 4 | Plots of highest occupied molecular orbital (HOMO) and lowest unoccupied molecular orbital (LUMO) of DB07107, DB06977, ST013616 and DB04200. The positive electron density has been shown in red color while negative have been shown in blue.

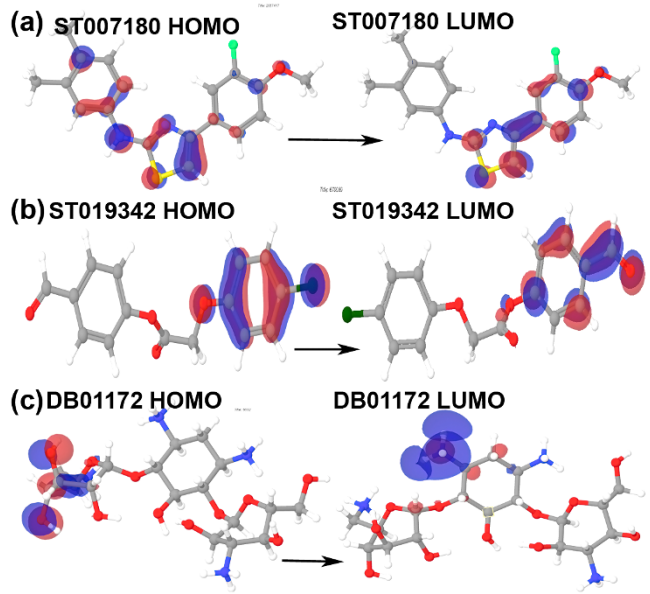

Figure 5 | Plots of highest occupied molecular orbital (HOMO) and lowest unoccupied molecular orbital (LUMO) ST007180, ST013942 and DB01172. The positive electron density has been shown in red color while negative have been shown in blue.

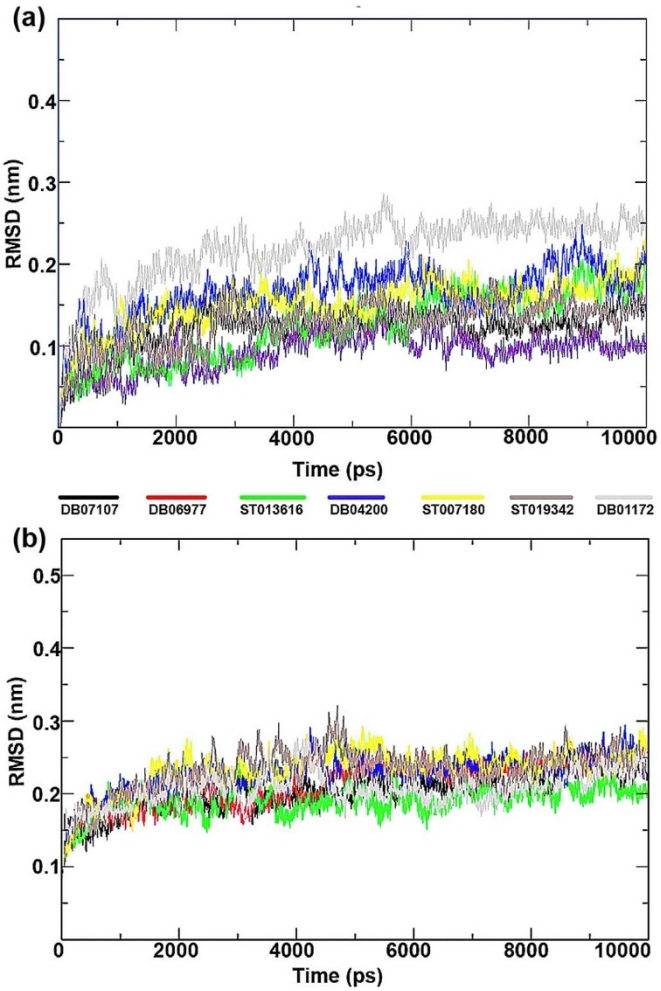

Figure 6 | Time dependence of root mean square deviations (RMSDs) of the Backbone of mutant (T3I51)and wild type of BCR-ABL have been shown in figure against the initial structure during 10,000 ps molecular dynamics (MD) simulation.

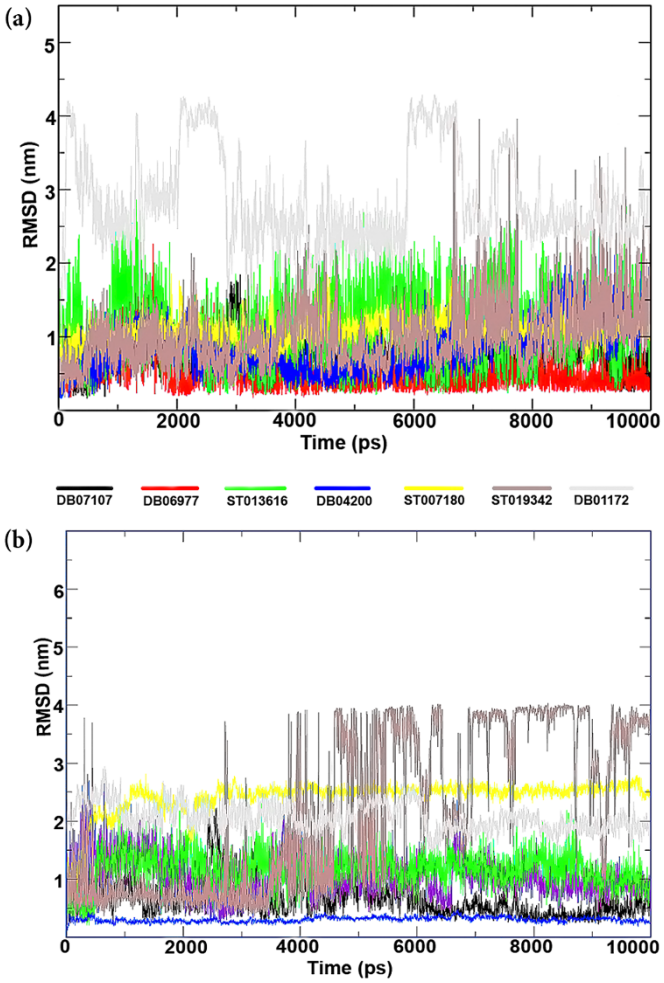

Figure 7 | Backbone RMSD values of drug candidates from both the types (wild and mutant) of protein ligand complexes were generated against the initial structures of protein-ligand complexes during 10,000 ps of molecular dynamics (MD) simulation period. Graphs were plotted using Xmgrace, a 3-D plotting tool.

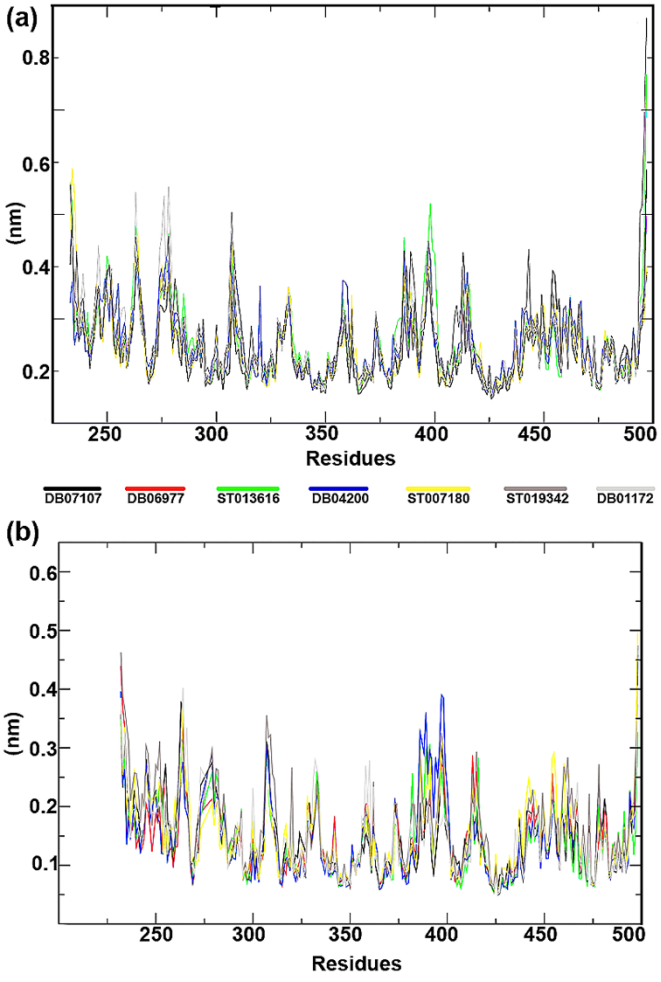

Figure 8 | Root mean square fluctuations (RMSF) from the initial structures of protein-ligand complexes during the trajectory period of simulation.

Interestingly, DB07107 ($C_{23}H_{22}N4O$) from DrugBank showed the highest binding energy with XP score of −14.045 kcal/mol (Figure 2a). To get an insight into their interacting pattern, we used UCFC Chimera molecular visualization tool and Glide for generating 2D interaction plots. Docking pose analysis revealed four hydrogen bonds (H_bonds) interactions with the ATP binding site residues of BCR-ABL. Here, we observed single H_bond with each Glu286 and Met318 residues with bond length of 2.92Å and 2.97Å while two H_bond formations were observed with Asp381 with the bond length of 3.32Å and 2.72Å.

Other potent drugs, DB06977 ($C_{23}H_{21}N5_O$), ST013616 ($C_{14}H_{12}N_4O_2$), DB04200 ($C_{20}H_{22}O_6$), ST007180 ($C_{18}H_{17}FN_2OS$), ST019342 ($C_{15}H_{11}C_lO_4$) (Figure 2b,2c,2d,2e,2f) and DB01172 ($C_{18}H_{36}N_4O_{11}$) (Figure 3) showed high binding affinity with XP scores of −13.163 kcal/mol, −12.065 kcal/mol, −12.041 kcal/mol, −11.555 kcal/mol, −11.033 kcal/mol and −8.433 kcal/mol, respectively (Table 2). Here, it is noticeable that the key residues of Glu286, Meth318 and Asp381 were involved in the H_bond interactions as has been observed with the marketed drug, ponatinib. Although DB01172 exhibits XP docking scored below the cuttoff value, we consider it as a potent inhibitor for BCR-ABL because it showed the highest number of H_bond with the hot spot residues of BCR-ABL. Moreover, it uncovered one side chain hydrogen bond with Glu282, Glu286, Asp381, Lys285 and one backbone hydrogen bond each with Asp381, Ile360. Therefore, we considered DB01172 for our further analysis.

Assessment of identified drugs in Wild-type of BCR-ABL. To determine the efficacy of the selected drug in binding to and inhibiting wild-type of BCR-ABL we performed docking studies as described in the methods section. To compare their efficacy and binding pattern with our screened compounds we again docked FDA approved drugs with wild-type of BCR-ABL.

As shown in table 2, DB07107 and DB06977 showed better docking scores than existing drugs while others showed results comparable to those of marketed drugs like ponatinib, bosutinib, bafetinib, dasatinib, nilotinib and imatinib. In the case of DB06977, although one H_bond is missing (Met318) with the wild-type of BCR-ABL complex compared to T315I mutant type, it still exhibits a favorable binding score of −10.94 kcal/mol. While, in the case of ST013616, one extra H_bond interaction is found to interact with Lys271. However, it did not show H-bond interaction with Asp381. Most of the selected drugs in these studies showed slightly less efficacy against wild-type compared to mutant BCR-ABL but better when compared to ponatinib. These investigations lead us to conclude that DB07107, DB06977, ST013616, DB04200 and ST007180 are more effective against the mutant than the wild-type BCR-ABL. ST019342, and DB01172 are effective only against mutant BCR-ABL.

DFT analysis. HOMO-LUMO plays an important role in stabilizing the interactions between drug and receptor protein[32]. Hence, the

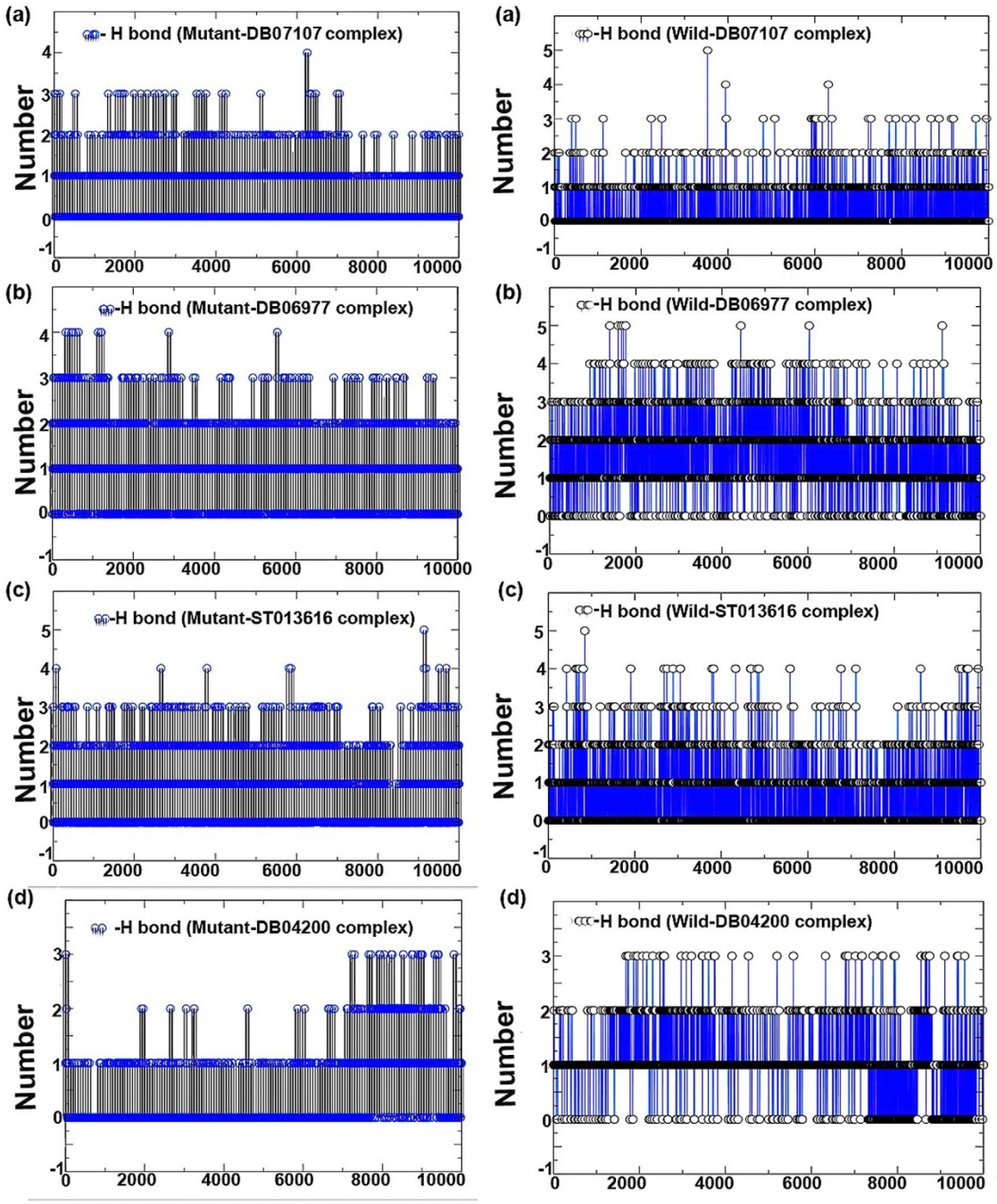

Figure 9 | Total number of inter-molecular H_bond interactions between the drug compounds (DB07107, DB06977, ST013616 and DB04200) and BCR-ABL (mutant and wild).

orbital energy of both HOMO and LUMO and the gap between them was calculated to estimate the chemical reactivity of the selected compounds using DFT (Table 3). HOMO-LUMO plots were generated to analyze the atomic contribution for these orbitals. The plots of HOMO and LUMO show the positive electron density in red color and negative electron density in blue (Figures 4 and 5). All the selected drug candidates showed minimal HOMO-LUMO gap with the average energy difference of 0.13 eV, signifying molecular reactivity. The lowest energy gap was exhibited by DB06977 with the HOMO-LUMO gap energy of 0.09911 eV and the highest energy gap was observed in DB04200 with the gap energy of 0.18442 eV (Table 3). HOMO energy was higher for DB07107 (Figure 4) and DB01172 (Figure 5), when compared to LUMO energy indicating an ability to donate the electrons rather than accept electrons with their partner receptor-binding site region.

Molecular dynamics simulations. To compare the structural behavior and flexibility of the wild-type and mutant BCR-ABL, all lead compounds were incorporated in Gromacs4.5.5 and MD was performed for 10 ns of each complexes. Root mean square deviations (RMSD) of the wild-type and mutant BCR-ABL were calculated against their initial structure in the protein-ligand complexes and graphs were generated to compare the flexibility of the backbone of the proteins using the Xmgrace software. Throughout the simulation period, no significant fluctuations were observed in the backbone of

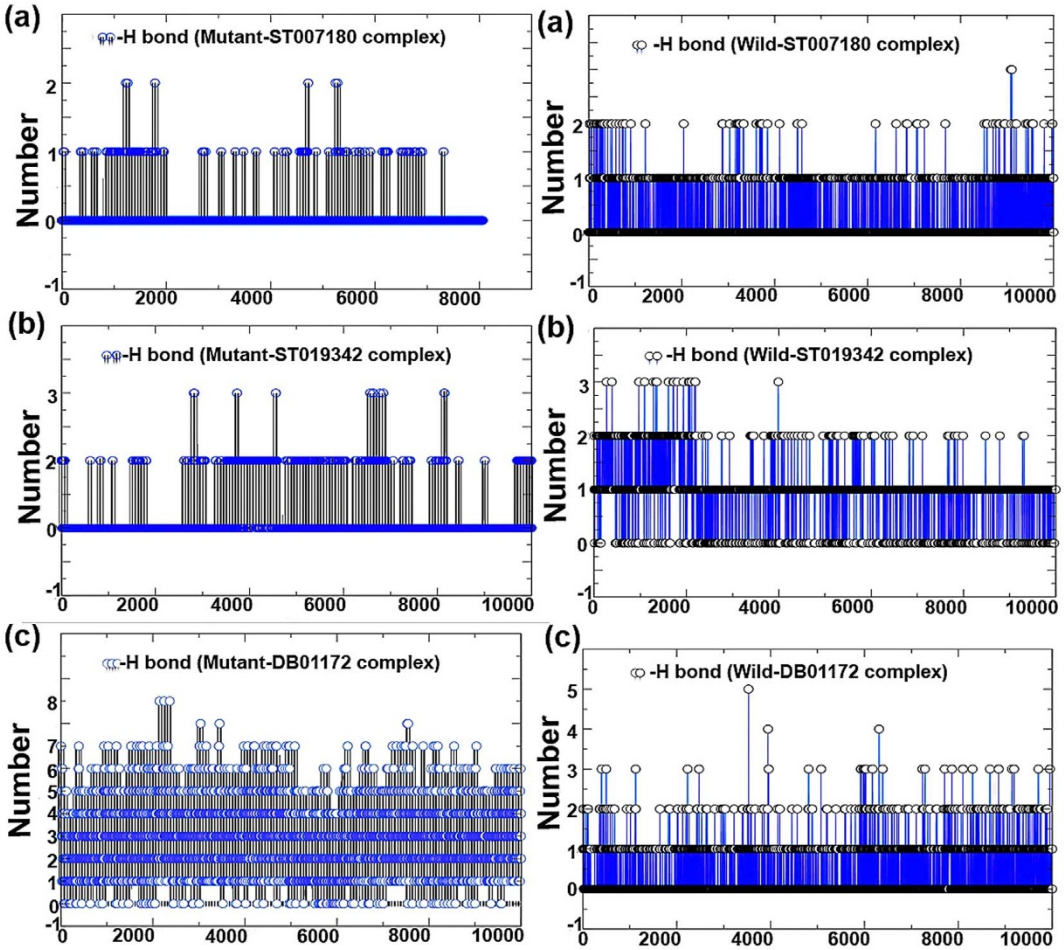

Figure 10 | Total number of inter-molecular H_bond interactions between BCR-ABL (mutant and wild) and ST007180, ST019342 and DB01172.

the wild-type and mutant T315I BCR-ABL, implying that the binding of drug candidates at the active site of the proteins is not only stable and strong but also does not disturb the protein backbone stability (Figure 6).

To ensure the binding stability of the drug candidates in the active site of proteins, ligand positional RMSD of each lead molecule were generated and analyzed as described study[41]. ST019342 showed more and continues fluctuations in the noticeable window size of 0.2–2.5 nm (Figure 7a) for wild-type and 0.2–4 nm for the mutant BCR-ABL complex (Figure 7b). Co-ordinates of ST019342-BCR-ABL (wild-type and mutant) complex were downloaded from the trajectory in the interval of 1000 ps and investigated in PyMOL for protein-ligand interactions. Our investigation uncovered that ST019342 has an unstable binding affinity towards BCR-ABL. It exhibits weak hydrogen bond interactions with the receptor binding site, which leads to the inefficient inhibition of BCR-ABL. Upon investigation of downloaded timeframe of MD, we observed that after 2 to 5 ns ST019342 was not bound to the binding pocket. It suggests its inability to inhibit the protein target efficiently while other drug candidates have shown stable and strong binding affinity.

In order to calculate the residual mobility of each lead molecules in BCR-ABL-ligand complexes (wild-type and mutant), Root Mean Square Fluctuation (RMSF) was calculated in each complexes and the graph was plotted against the residue number based on the trajectory period of MD simulation. None of the drug candidates showed noticeable changes in their residual level as the general profile of residual fluctuation of wild-type and T315I is minimal in each complex without any abnormal fluctuation (Figure 8).

Hydrogen bond analysis. To determine the stability of hydrogen bonds with the ATP binding site of protein, MD analysis of BCR-ABL and the selected drug candidate's complex stability were monitored during the trajectory period. Hydrogen bond profiles between the selected drugs and BCR-ABL (T315I and wild-type) were calculated using the g_hbond utility of GROMACS. This analysis revealed that DB01172 comprises 6–7 (highest) average H_bonds during the simulation period sharing four H_bonds with Glu282, Lys285, Glu286 and Ile360, and two H_bonds with Asp381 (Figures 9 and 10) in T315I (mutant) while Wild-type showed poor H_bond interactions with 1–2 H_bonds on average during the trajectory period. The same pattern was also observed in the case of ST007180 and ST019342. ST007180 and ST019342 showed less number of hydrogen bond plots in the mutant BCR-ABL compared to wild type. To gain insight into the hydrogen bond instability, we downloaded the drug-receptor complexes in the interval of one ns for DB01172, ST007180 and ST019342. Following which, the structures were superimposed to monitor the binding pose of the drug candidates throughout the trajectories. Our investigation revealed that DB01172 is moving away from the ATP binding site of BCR-ABL in both mutant and wild-type towards the north-west (130°) and east direction (180°) (Figure 11). Compound ST007180 showed satisfactory results, while ST019342 showed slight movement in the binding site.

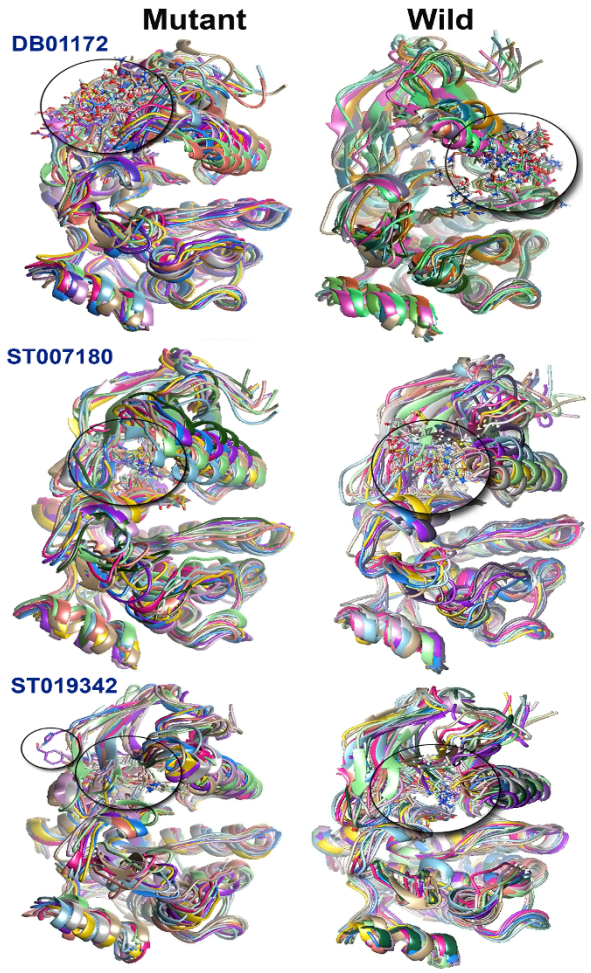

Figure 11 | Spnapshot of the superimposed structures of mutant and wild type of DB01172 and ST007180 and ST019342. Stuctures were downloaded from the trajectory file in the interval of 1 ns.

Other complexes, DB07107, DB06977, ST013616 and DB04200 exposed an average number of hydrogen bonds 2–3 (Glu286, Met318 and Asp381), 3 (Glu286, Met318 and Asp381), 3–4 (Glu286, Asp381, Glu316, Met318), 2–3 (Glu286 and Met318), 1 (322) and 1–2 (Met318 and Asn322), respectively in both wild-type and mutant BCR-ABL. The average number of H_bonds throughout the MD period signifies their continuous contribution in H_bond interactions, which provides stability to the complexes in holding it to the ATP binding position. This suggests that the functionality and ability of these compounds can efficiently inhibit BCR-ABL.

Interaction energy and binding free energy. To estimate the binding association between wild-type and mutant of BCR-ABL, two different approaches were carried out. Firstly, crude interaction energy was estimated based on the short-range energy of the system. Next, to determine the binding affinity between BCR-ABL and drug complexes we scored the MM-GBSA energy of the complexes. Interaction energy data suggests that all the selected drug compounds have higher interaction energy of 203444.3 kcal/mol, −203449.57 kcal/mol, −292066.20 kcal/mol, −310571.94 kcal/mol, −295967.25 kcal/mol, −292055.68 kcal/mol, −292134.56 kcal/mol in DB07107, DB06977, ST013616, DB04200, ST007180, ST019342, and DB01172 respectively, for the mutant than wild-type which showed −232088.91 kcal/mol, −232068.12 kcal/mol, −232062.86 kcal/mol, −232033.94 kcal/mol, −232030.35 kcal/mol, −232091.54 kcal/mol, and −232062.86 kcal/mol for DB07107, DB06977, ST013616, DB04200, ST007180, ST019342, and DB01172 respectively (Table 4).

Re-scoring of complexes using Prime MM-GBSA results indicated that all the selected drug candidates displayed higher binding free energy (Table 4). Moreover, all of them displayed results ideal for being a drug candidate in the treatment of CML bearing wild-type or mutant BCR-ABL. Our studies show that these drugs can efficiently inhibit BCR-ABL by binding to DFG out conformation of BCR-ABL protein and can obstruct its catalytic activity. Hence, we recommend DB07107, DB06977, ST013616, DB04200 and ST007180 to be experimentally tested and further authenticated. Since ST019342 and DB01172 are not recommended in the broad-spectrum purpose due to their unbalanced backbone conformation in wild-type during the MD study, we recommend for further experimentation and use against T315I. The entire work flow chart of this study is shown in Figure 12.

Conclusions

Using a virtual screening approach, we performed a molecular docking study for both wild-type and mutant (T315I) of BCR-ABL. The study yielded seven lead molecules which showed promising results

Table 4 | Interactions energy and binding free energy of mutant and wild-type of BCR-ABL-ligand complexes

Ligand	Average[a]	Average (wild-type)	Int. energy[a] (Kcal/mol)	Int. energy[b] (Kcal/mol)	MM-GBSA[a]	MM-GBSA[b]
DB07107	159619 LJ (SR) −1.01083e + 06 Q(SR)	184840 LJ (SR) −1.1559e + 06 Q (SR)	−203444.31	−232088.91	−112.76	−112.25
DB06977	159597 LJ (SR) −1.01083e + 06 Q(SR)	184807 LJ (SR) −1.15578e + 06 Q (SR)	−203449.57	−232068.12	−126.71	−124.78
ST013616	237095 LJ(SR) −1.4591e + 06 Q(SR)	184949 LJ (SR) −1.1559e + 06 Q (SR)	−292066.20	−232062.86	−71.53	−82.32
DB04200	159667 LJ (SR) −1.4591e + 06 Q(SR)	184780 LJ (SR) - −1.15561e + 06 Q (SR)	−310571.94	−232033.94	−103.15	−103.08
ST007180	243003 LJ(SR) −1.48133e + 06 Q(SR)	184855 LJ (SR) −1.15567e + 06 Q (SR)	−295967.25	−232030.35	−93.59	−81.26
ST019342	237089 LJ (SR) −1.45905e + 06 Q(SR)	184879 LJ (SR) −1.15595e + 06 Q (SR)	−292055.68	−232091.54	−73.73	−75.83
DB01172	237089 LJ(SR) −1.45938e + 06 Q(SR)	184949 LJ (SR) −1.1559e + 06 Q (SR)	−292134.56	−232062.86	−83.82	−72.25

[a]: mutant.
[b]: wild-type.

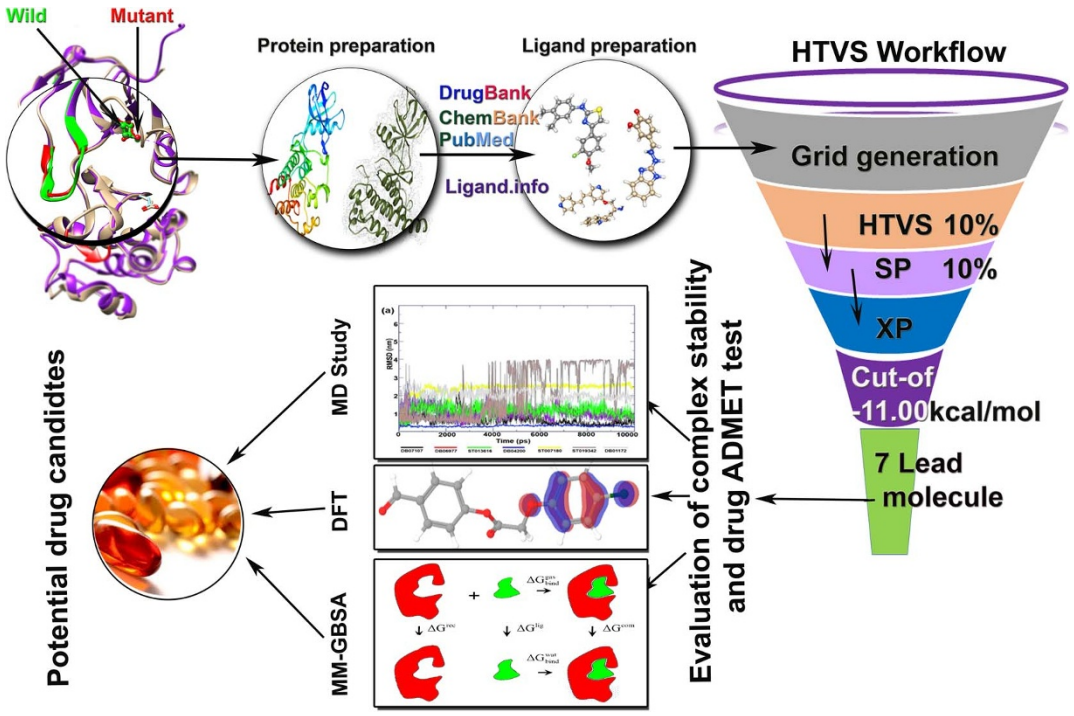

Figure 12 | **Graphical abstract.**

against both wild-type and T315I mutant BCR-ABL. The bioactivity of these selected lead compounds were determined using frontier orbital study and the results showed that the selected drug candidates are chemically reactive. The stability of the protein-ligand complexes were investigated through 10 ns of MD simulation of each complex for both types. MD simulation studies illustrated the dynamic behavior of protein-ligand complexes. Results showed that the protein backbone and ligand backbone of DB07107, DB06977, ST013616, DB04200, ST007180 and DB01172 compounds are stable throughout the simulation period without any significant fluctuation within this period. In contrast, backbone of ST019342 showed anomalous fluctuations throughout the simulation period while DB01172 showed instability in RMSD graph with the wild-type BCR-ABL. Hydrogen bond analysis revealed that DB01172 has six hydrogens on average, while in wild-type it has 2–3 on average, implying low efficacy towards the wild-type of target. Therefore, in terms of broad spectrum therapy for CML ST019342 and DB01172 drugs are not recommended while DB07107, DB06977, ST013616, DB04200 and ST007180 showed remarkable results during the trajectory period. These drugs promise a new gateway for the further development of anti CML therapeutics targeting BCR-ABL. In summary, DB07107, DB06977, ST013616, DB04200 and ST007180 are more effective in inhibiting mutant than wild-type of BCR-ABL. ST019342 and DB01172 are effective only in mutant BCR-ABL.

1. Quintas-Cardama, A. & Cortes, J. Molecular biology of bcr-abl1-positive chronic myeloid leukemia. *Blood.* **113**, 1619–1630 (2009).
2. Pendergast, A. M. *et al.* BCR-ABL-induced oncogenesis is mediated by direct interaction with the SH2 domain of the GRB-2 adaptor protein. *Cell.* **75**, 175–185 (1993).
3. Deininger, M. W., Goldman, J. M. & Melo, J. V. The molecular biology of chronic myeloid leukemia. *Blood.* **96**, 3343–3356 (2000).
4. Capdeville, R., Buchdunger, E., Zimmermann, J. & Matter, A. Glivec (STI571, imatinib), a rationally developed, targeted anticancer drug. *Nat Rev Drug Discov.* **1**, 493–502 (2002).
5. O'Hare, T., Eide, C. A. & Deininger, M. W. Bcr-Abl kinase domain mutations, drug resistance, and the road to a cure for chronic myeloid leukemia. *Blood.* **110**, 2242–2249 (2007).
6. Weisberg, E. *et al.* Characterization of AMN107, a selective inhibitor of native and mutant Bcr-Abl. *Cancer Cell.* **7**, 129–141 (2005).
7. Sawyers, C. L. Even better kinase inhibitors for chronic myeloid leukemia. *N. Engl. J. Med.* **362**, 2314–2315 (2010).
8. O'Hare, T. *et al.* In vitro activity of Bcr-Abl inhibitors AMN107 and BMS-354825 against clinically relevant imatinib-resistant Abl kinase domain mutants. *Cancer Res.* **65**, 4500–4505 (2005).
9. Deguchi, Y. *et al.* Comparison of imatinib, dasatinib, nilotinib and INNO-406 in imatinib-resistant cell lines. *Leukemia Res.* **32**, 980–983 (2008).
10. Redaelli, S. *et al.* Activity of bosutinib, dasatinib, and nilotinib against 18 imatinib-resistant BCR/ABL mutants. *J. Clin. Oncol.* **27**, 469–471 (2009).
11. O'Hare, T. *et al.* AP24534, a pan-BCR-ABL inhibitor for chronic myeloid leukemia, potently inhibits the T315I mutant and overcomes mutation-based resistance. *Cancer Cell.* **16**, 401–412 (2009).
12. O'Hare, T. *et al.* Inhibition of wild-type and mutant Bcr-Abl by AP23464, a potent ATP-based oncogenic protein kinase inhibitor: implications for CML. *Blood.* **104**, 2532–2539 (2004).
13. Frankfurt, O. & Licht, J. D. Ponatinib--a step forward in overcoming resistance in chronic myeloid leukemia. *Clin Cancer Res.* **19**, 5828–5834 (2013).
14. Reddy, E. P. & Aggarwal, A. K. The ins and outs of bcr-abl inhibition. *Genes & cancer.* 3, 447–454 (2012).
15. Ariad suspends ponatinib sales. *Cancer Discov.* **4**, 6–7 (2014).
16. Zhou, T. *et al.* Structural mechanism of the Pan-BCR-ABL inhibitor ponatinib (AP24534): lessons for overcoming kinase inhibitor resistance. *Chem Biol Drug Des.* **77**, 1–11 (2011).
17. Chan, W. W. *et al.* Conformational control inhibition of the BCR-ABL1 tyrosine kinase, including the gatekeeper T315I mutant, by the switch-control inhibitor DCC-2036. *Cancer Cell.* **19**, 556–568 (2011).
18. Banks, J. L. *et al.* Integrated Modeling Program, Applied Chemical Theory (IMPACT). *J. Comput. Chem.* **26**, 1752–1780 (2005).
19. von Grotthuss, M., Pas, J. & Rychlewski, L. Ligand-Info, searching for similar small compounds using index profiles. *Bioinformatics.* **19**, 1041–1042 (2003).
20. von Grotthuss, M., Koczyk, G., Pas, J., Wyrwicz, L. S. & Rychlewski, L. Ligand.Info small-molecule Meta-Database. *Comb Chem High Throughput Screen.* **7**, 757–761 (2004).
21. Knox, C. *et al.* DrugBank 3.0: a comprehensive resource for 'omics' research on drugs. *Nucleic Acids Res.* **39**, D1035–1041 (2011).
22. Wishart, D. S. *et al.* DrugBank: a knowledgebase for drugs, drug actions and drug targets. *Nucleic Acids Res.* **36**, D901–906 (2008).
23. Evan E. Bolton., Y. W., Paul A. Thiessen. & Stephen H. Bryant. PubChem: Integrated Platform of Small Molecules and Biological Activities. *Annu Rep Comput Chem.* **4**, 217–240 (2008).
24. Greenwood, J. R., Calkins, D., Sullivan, A. P. & Shelley, J. C. Towards the comprehensive, rapid, and accurate prediction of the favorable tautomeric states

of drug-like molecules in aqueous solution. *J. Comput. Aided Mol. Des.* **24**, 591–604 (2010).
25. Shelley, J. C. *et al.* Epik: a software program for pK(a) prediction and protonation state generation for drug-like molecules. *J. Comput. Aided Mol. Des.* **21**, 681–691 (2007).
26. Friesner, R. A. *et al.* Extra precision glide: docking and scoring incorporating a model of hydrophobic enclosure for protein-ligand complexes. *J Med Chem.* **49**, 6177–6196 (2006).
27. Matysiak, J. Evaluation of electronic, lipophilic and membrane affinity effects on antiproliferative activity of 5-substituted-2-(2,4-dihydroxyphenyl)-1,3,4-thiadiazoles against various human cancer cells. *Eur. J. Med. Chem.* **42**, 940–947 (2007).
28. Becke, A. D. Density-functional thermochemistry. III. The role of exact exchange. *J. Chem. Phys.* **98**, 5648–5652 (1993).
29. Gill, P. M. W., Johnson, B. G., Pople, J. A. & Frisch, M. J. The performance of the Becke—Lee—Yang—Parr (B—LYP) density functional theory with various basis sets. *Chem. Phys. Lett.* **197**, 499–505 (1992).
30. Stephens, P. J., Devlin, F. J., Chabalowski, C. F. & Frisch, M. J. Ab Initio Calculation of Vibrational Absorption and Circular Dichroism Spectra Using Density Functional Force Fields. *J. Phys. Chem.* **98**, 11623–11627 (1994).
31. Zhan, C.-G., Nichols, J. A. & Dixon, D. A. Ionization Potential, Electron Affinity, Electronegativity, Hardness, and Electron Excitation Energy: Molecular Properties from Density Functional Theory Orbital Energies. *J. Phys. Chem. A.* **107**, 4184–4195 (2003).
32. Zheng, Y. *et al.* Design, synthesis, quantum chemical studies and biological activity evaluation of pyrazole-benzimidazole derivatives as potent Aurora A/B kinase inhibitors. *Bioorg. Med. Chem. Lett.s.* **23**, 3523–3530 (2013).
33. Pronk, S. *et al.* GROMACS 4.5: a high-throughput and highly parallel open source molecular simulation toolkit. *Bioinformatics.* **29**, 845–854 (2013).
34. Sharma, O. P., Vadlamudi, Y., Liao, Q. H., Strodel, B. & Kumar, M. S. Molecular modeling, dynamics, and an insight into the structural inhibition of cofactor independent phosphoglycerate mutase isoform 1 from Wuchereria bancrofti using cheminformatics and mutational studies. *J Biomol Struct Dyn.* **31**, 765–778 (2013).
35. Malde, A. K. *et al.* An Automated Force Field Topology Builder (ATB) and Repository: Version 1.0. *J. Chem. Theory Comput.* **7**, 4026–4037 (2011).
36. Oostenbrink, C., Villa, A., Mark, A. E. & van Gunsteren, W. F. A biomolecular force field based on the free enthalpy of hydration and solvation: the GROMOS force-field parameter sets 53A5 and 53A6. *J. Comput. Chem.* **25**, 1656–1676 (2004).
37. Wang, H., Dommert, F. & Holm, C. Optimizing working parameters of the smooth particle mesh Ewald algorithm in terms of accuracy and efficiency. *J Chem Phys.* **133**, 034117 (2010).
38. Amiri, S., Sansom, M. S. & Biggin, P. C. Molecular dynamics studies of AChBP with nicotine and carbamylcholine: the role of water in the binding pocket. *Protein Eng Des Sel.* **20**, 353–359 (2007).
39. Pettersen, E. F. *et al.* UCSF Chimera--a visualization system for exploratory research and analysis. *J. Comput. Chem.* **25**, 1605–1612 (2004).
40. Lyne, P. D., Lamb, M. L. & Saeh, J. C. Accurate prediction of the relative potencies of members of a series of kinase inhibitors using molecular docking and MM-GBSA scoring. *J Med Chem.* **49**, 4805–4808 (2006).
41. Sharma, O. P. *et al.* Modeling, docking, simulation, and inhibitory activity of the benzimidazole analogue against beta-tubulin protein from Brugia malayi for treating lymphatic filariasis. *Med Chem Res.* **21**, 2415–2427 (2012).

Acknowledgments

The research work was carried out in the laboratory of the Centre for Excellence in Bioinformatics, and Department of Biochemistry & Molecular Biology, Pondicherry University-India. Hemanth Naick thanks Pondicherry University and UGC-BSR Research fellowship for the financial assistant. Om Prakash Sharma is grateful to the Council of Scientific & Industrial Research (CSIR), India for the Senior Research Fellowship (09/559/(0085)/2012/EMR-I) to pursue their Ph.D. degree.

Author contributions

H.N., O.P. and R.B. conceived the study. H.N. and O.P. performed the model output analysis and wrote the initial draft of the paper. H.N., O.P., M.S.K. and R.B. contributed to interpreting results, discussion of the associated dynamics, and improvement of this paper.

Additional information

Competing financial interests: The authors declare no competing financial interests.

How to cite this article: Banavath, H.N., Sharma, O.P., Kumar, M.S. & Baskaran, R. Identification of novel tyrosine kinase inhibitors for drug resistant T315I mutant BCR-ABL: a virtual screening and molecular dynamics simulations study. *Sci. Rep.* **4**, 6948; DOI:10.1038/srep06948 (2014).